Wear 376-377 (2017) 549–556

Contents lists available at ScienceDirect

Wear

journal homepage: www.elsevier.com/locate/wear

Erosion-corrosion of X-52 steel pipe under turbulent swirling impinging jets

C. Sedano-de la Rosa [a,*], M. Vite-Torres [a], J.G. Godínez-Salcedo [b], E.A. Gallardo-Hernández [a], R. Cuamatzi-Melendez [c], L.I. Farfán-Cabrera [a]

[a] Instituto Politécnico Nacional, SEPI-ESIME-UZ, Grupo de Tribología Col. Lindavista, C.P. 07320 Ciudad de México, Mexico
[b] Instituto Politécnico Nacional, ESIQIE, C.P. 07738 Ciudad de México, Mexico
[c] Instituto Mexicano del Petroleo, Col. San Bartolo Atepehuacan, CP 07730 Cd. de México, Mexico

ARTICLE INFO

Article history:
Received 12 September 2016
Received in revised form
11 December 2016
Accepted 21 December 2016

Keywords:
Turbulent swirling impinging jet
Swirl number
Erosion-corrosion
X-52 steel pipe
Polarization resistance

ABSTRACT

Erosion-corrosion tests were carried out at two regimes, non-swirling jets with swirl number (S=0), and weakly swirling jets up to reaching vortex breakdown (S=0.1, 0.2 and 0.3); the average flow velocity was adjusted at 3.2 ms^{-1}, meanwhile the corrosive media consisted of 1 l of distilled water and 2 g/l NaCl purged with CO_2 and abrasive particles of 20 μm of aluminium oxide (Al_2O_3) suspended into test solution with a content of 11 kg m^{-3}. The impinging angle was 90 ° in the near-field. Electrochemical measurements were performed using the polarization resistance technique (Rp). Furthermore, to characterize the damaged surface, optical and scanning electron microscopy (SEM) images were taken, also the corrosion products were analyzed by means of X-ray diffraction (XRD) and EDS techniques to identify the material loss mechanism. The experimental results shows that the maximum corrosion rate was observed at high swirl numbers, moreover, this swirling regime is more severe than the non-swirling condition improving the pit formation.

1. Introduction

The erosion-corrosion phenomenon causes wear when abrasive particles are present into a liquid solution for instance water; it caused by the relative movement of the solids with respect to the surface. Such wear is more prevalent where fluid is forced to change direction or where high shear stresses occur. Basically the particles must penetrate the laminar sublayer with enough force to remove the passive film on the alloy. For this reason, high shear stresses are often required. The above situation can cause significant damage in systems carrying saltwater and solids, for example, carbon steel carrying air plus particles [1]. In recent investigations, the erosion-corrosion behaviour has been characterized using different techniques, for instance the submerged jet impingement [2–5], the slurry pot erosion tester [6], the rotating disk electrode [7], as well as the close loop technique [8–11].

On the other hand, the API 5L X52 low carbon steel pipe, is typically used for the conduction of gas and fuel in large volumes over long distances in the petroleum industry, due to its high mechanical resistance and well response when is exposed to different aggressive environments [12,13]. Tests have been developed in different environments [13–17] such as Corrosion inhibitors, H_2SO_4, neutral and high pH, and CO_2-Saturated NaCl in brine media.

In addition, swirling flows have achieved better technical applications, for example in cyclone separators, burners, propellers, dredges, excavators, etc. While, the rotating jet is a fluid stream forced by pressure of an opening or nozzle, where a tangential velocity is superimposed on the axial flow in a circular jet, both radial and axial pressure gradients are generated. These gradients may significantly influence the flow changing the geometry, the evolution and the interactions between the vortical structures. For swirling jets different flow regimes may be identified depending on the degree of swirl present in the jet [18]. There are different definitions of swirl number or swirl intensity, S, the most often used one is the proposed by Beer and Chigier [19] and used by Wu et al. [20], and is defined as the ratio of axial flux of angular momentum to the axial flux of the axial momentum.

$$S = M_{angular}/RM_{axial} = \int_0^R U_{axial}U_{tangential}r^2dr/R\int_0^R U_{axial}^2 rdr \quad (1)$$

Where $U_{tangential}$ is the characteristic tangential velocity, U_{axial} is axial velocity, $M_{angular}$ is axial flux of angular momentum, M_{axial} is axial flux of axial momentum, and R is the inlet radius.

In some publications [21–27], this type of flow has been studied particularly with applications on cavitation reactors, heat transfer distribution, flame jets, gas turbine blades, acceleration and

* Corresponding author.
E-mail address: cesar_sedano@prodigy.net.mx (C. Sedano-de la Rosa).

http://dx.doi.org/10.1016/j.wear.2016.12.063
0043-1648/

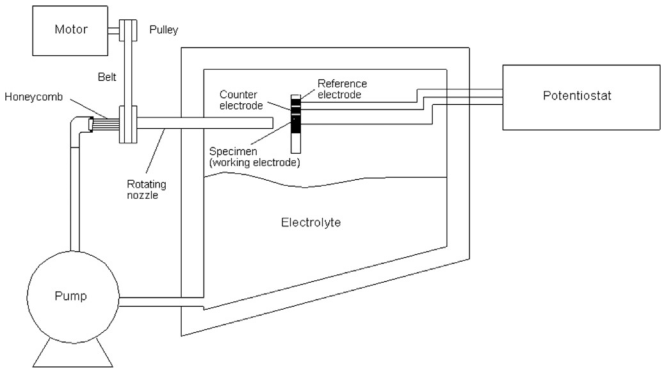

Fig. 1. Schematic diagram of the erosion-corrosion rig developed.

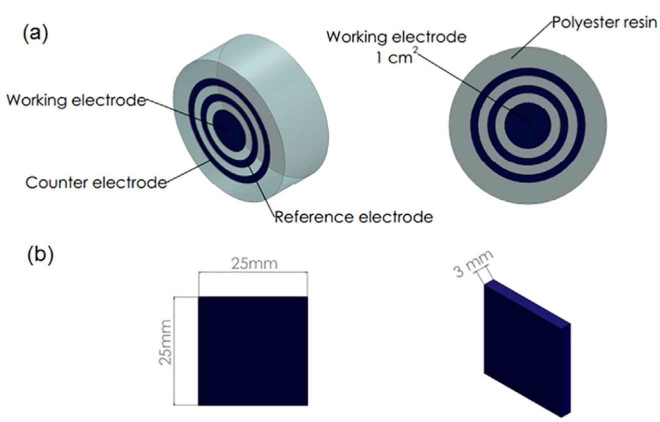

Fig. 2. (a) Specimens for electrochemical measurements; (b) Specimens for surface damage and corrosion products characterization.

penetration of micro-particles, excavation and pipeline flows. In addition, some researchers [28] have conducted erosion-corrosion experiments at submerged conditions; nevertheless, an impinging jet can be classified as a) Submerged Jet or b) Free Jet; if the fluid issuing from the nozzle is of the same density and nature as that of the surrounding fluid, then the jet is called a Submerged Jet. On the contrary if it has different density than the surrounding fluid then is called a Free Jet. When the jet is submerged, the turbulence induced due to shear layer is carried toward the centre of the jet. On the opposite, if the jet is free, this effect is not so prominent [29]. The range of materials used on the tester, could be metals and its alloys susceptible to erosion-corrosion damage, for example carbon steel, stainless steel, aluminum, lead, copper, among others [30]. The aim of this work is to gain knowledge of erosion-corrosion wear behaviour on API 5L X-52 carbon steel, under swirling and non-submerged jet conditions not yet implemented in tribological tests.

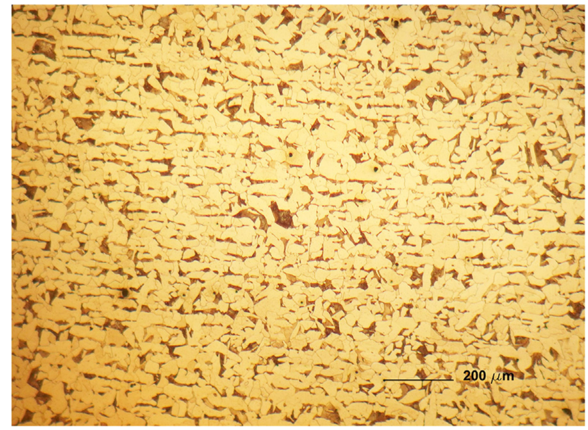

Fig. 3. Bright field optical image of API 5L X-52 steel microstructure, etched with Nital 2%.

Table 2
Operating conditions for erosion-corrosion of API 5L X-52 steel.

Nozzle diameter	6.35 mm
Standoff distance	6.35 mm
Test media	Distilled water + 2 g/l of NaCl + 11 kgm^{-3} of 20 μm Al_2O_3
Test duration	1 h, 2 h, 3 h and 4 h
Test temperature	Room temperature
Angle of incidence	90°
Swirl number (S)	0, 0.1, 0.2, and 0.3
Average flow velocity	3.2 m s^{-1}

2. Experimental

2.1. Experimental set-up

The erosion-corrosion tester was designed to control and adjust nozzle rotation frequency, flow velocity, specimen distance and orientation relative to the impinging stream. Fig. 1, shows the schematic diagram of the developed rig, manufactured by IPN-SEPI-ESIME-Zacatenco, Tribology Group. This equipment was designed considering a few aspects on wear corrosion phenomenon mentioned in the G119 ASTM Standard [31,32].

The nozzle has an inner diameter of 6.35 mm, turned by means of an AC motor through a pulley and belt system. The impinging angle employed was 90° in the near field, that is the standoff distance was 6.35 mm, equal to the nozzle inner diameter. A 20 mm high honeycomb section with grid diameter of 2.38 mm, is fitted inside the straight nozzle tube to produce the rotation movement of the solid-body [33]. The electrolyte consists of 1 l of distilled water with 2 g/l of NaCl and saturated with CO_2 to reach a pH of 3.86 before the experiments, additionally abrasive particles of 20 μm of Al_2O_3 were suspended with a content of 11 kgm^{-3} to generate the erosion-corrosion wear. Besides, two different configurations of specimens were used; a probe arrangement with three-electrode concentric rings was used for electrochemical

Table 1
Physical and chemical properties of API 5L X-52 steel.

Yield strength			429 MPa						
Density			7.82 g cm^{-3}						
Equivalent weight			18.62 g						
Hardness			197 HV0.1						
Composition (%)									
Fe	C	Si	Mn	P	S	Cr	Nb	Ti	V
98.3	0.075	0.194	0.675	0.0754	0.047	0.0118	0.0354	0.0075	0.003